

A New Method for Measuring Edge Tensions and Stability of Lipid Bilayers: Effect of Membrane Composition

Thomas Portet^{†‡} and Rumiana Dimova^{†*}

[†]Institut de Pharmacologie et de Biologie Structurale and Laboratoire de Physique Théorique, Université Paul Sabatier, CNRS, Toulouse, France; and [‡]Max Planck Institute of Colloids and Interfaces, Potsdam, Germany

ABSTRACT We report a novel and facile method for measuring edge tensions of lipid membranes. The approach is based on electroporation of giant unilamellar vesicles and analysis of the pore closure dynamics. We applied this method to evaluate the edge tension in membranes with four different compositions: egg phosphatidylcholine (eggPC), dioleoylphosphatidylcholine (DOPC), and mixtures of DOPC with cholesterol and dioleoylphosphatidylethanolamine. Our data confirm previous results for eggPC and DOPC. The addition of 17 mol % cholesterol to the DOPC membrane causes an increase in the membrane edge tension. On the contrary, when the same fraction of dioleoylphosphatidylethanolamine is added to the membrane, a decrease in the edge tension is observed, which is an unexpected result considering the inverted-cone shape geometry of the molecule. It is presumed that interlipid hydrogen bonding is the origin of this behavior. Furthermore, cholesterol was found to lower the lysis tension of DOPC bilayers. This behavior differs from that observed on bilayers made of stearyl dioleoylphosphatidylcholine, suggesting that cholesterol influences the membrane mechanical stability in a lipid-specific manner.

INTRODUCTION

Spontaneous pore formation is suppressed in biological membranes, so that they can fulfill their role as a barrier. When a membrane is porated due to some external perturbation, lipid molecules reorient so that their polar heads can line the pore walls and form a hydrophilic pore (1). This rearrangement is energetically favorable, because it shields the hydrophobic tails from exposure to water. However, there is a price to pay for reorganizing the lipids at the pore edge. The energy penalty per unit length of pore circumference is called edge tension and is on the order of several piconewtons (2). The edge tension emerges from the physicochemical properties and the amphiphilic nature of lipid molecules, and it gives rise to a force driving the closure of transient pores (3).

In some reports, the edge tension is referred to as line tension. The latter term is presumably more appropriate for describing, for example, the tension along the borders of domains in multicomponent membranes. In porated bilayers, we will refer to the tension along the pore edge as edge tension.

The edge tension is of significant importance in biology. It contributes to the autoassembly and autohealing of lipid bilayer structures, which enable compartmentalization in cells needed for life to develop. Edge tension has been found to govern the stability of detergent-stabilized bicelles and to regulate the disc-to-vesicle transitions in such systems (4). It also plays a crucial role in membrane resealing mechanisms after physical protocols for drug delivery, such as sonoporation (5) or electroporation (6). Being able to experimentally measure this quantity is thus of significant interest for

understanding various biological events and physicochemical processes in membranes. Studies based on molecular dynamics simulation have also been able to deduce membrane edge tensions (7–9).

Only a few experimental methods have been developed to directly assess the membrane edge tension. Here, we give a short overview of the available approaches and their advantages and briefly outline the disadvantages. One of the main hurdles in measuring edge tension lies in visualizing the pores in the membrane. Indirect methods based on measuring properties statistically averaged over populations of small vesicles provide a possible solution, as reported, for example, in studies on osmotically induced leakage of vesicles (10). However, in such measurements the use of highly concentrated salt solutions influences significantly the membrane material properties (11). Another approach was based on rapid freezing of cells with a controlled time delay after electroporation, then examining the pores with electron microscopy (12). This method, however, provides a static picture of the porated membrane, and there is a risk of ice crystal damage to the cells. Another way to probe the edge energy, this time on supported lipid bilayers, is provided by a punch-through approach with an atomic force microscope (AFM) (13), but here, the support may influence the membrane behavior. Measurements of the voltage dependence of the average lifetime of pores in electroporated black lipid membranes also can be used to roughly estimate the edge tension (14,15). However, these membranes are at high tension and organic solvents may still be present in the bilayer.

The above-listed approaches and systems do not allow access to the pore dynamics, nor can the pores be directly observed by using them. A more convenient system, which provides a solution to this problem, is giant unilamellar

Submitted June 22, 2010, and accepted for publication September 16, 2010.

*Correspondence: Rumiana.Dimova@mpikg.mpg.de

Editor: Lukas K. Tamm.

© 2010 by the Biophysical Society
0006-3495/10/11/3264/10 \$2.00

doi: 10.1016/j.bpj.2010.09.032

vesicles (GUVs) (16). Because they have the dimensions of eukaryotic cells, GUVs can be visualized under an optical microscope and offer a convenient tool for studying membrane properties (17).

Only a few previous studies have employed GUVs for estimating the edge tension. Observations on open cylindrical giant vesicles exposed to AC fields (18) provided an estimate for the edge tension, but this technique could be applied to only a few (three) vesicles. In another work, the vesicles were porated with an electric pulse, and the pores were kept open by externally adjusting the membrane tension with a micropipette (19). This approach nevertheless requires the use of sophisticated equipment, such as a setup for vesicle micropipette aspiration. Another approach was the use of giant liposomes (20–22), where the pore closure dynamics was analyzed in light of a theory developed earlier by Brochard-Wyart et al. (3). However, it was necessary to use viscous media (glycerol solutions) and fluorescent dyes in the membrane for direct visualization of pore closure, and both of these agents may influence the edge tension. Indeed, glycerol is known to interact with phosphatidylcholine membranes via preferential exclusion from the hydration layer and membrane partitioning (23). It is thus conceivable that glycerol can influence the edge tension, because the latter depends on the repulsion between the lipid headgroups and the conformation of the hydrocarbon chains, as shown by simulation studies (24). On the other hand, the use of fluorescent dyes (21) to visualize the vesicles also can influence the measurements of edge tension because of preferential partitioning of the dye between the pore edges and the rest of the bilayer.

As done in other studies (20,21), we use the theoretical framework developed by Brochard-Wyart et al. (3), which describes pore dynamics. The principle of our method is simple. As in Brochard-Wyart et al. (3), one has to create a pore and measure its closure rate, which can be related to the edge tension. Porating a lipid bilayer can be carried out by applying tension to the membrane. Once the membrane tension exceeds a critical value called the lysis tension (2), the vesicle ruptures and a transient pore can appear. Karatekin et al. used visible light illumination to stretch the vesicles (21). However, when working with fluorescently labeled membranes, as in Karatekin et al. (21), there is a danger that intense illumination may trigger oxidation processes in the bilayer (25,26). Sandre et al. employed adhesion of the GUVs to a glass substrate (20), but this approach does not allow control over the location and initiation of the poration process.

Here, as in Zhelev and Needham (19), we use an electric pulse to generate micron-sized pores in the membrane. We observe the pore closure under phase-contrast microscopy using fast digital imaging. Thus, the need to use viscous solutions to slow down the system dynamics was avoided, and no fluorescent dyes were employed to visualize the vesicles. The pores close within a few tens or hundreds of

milliseconds, giving edge tensions of the order of several piconewtons, in agreement with values reported in the literature. We study the influence of membrane composition and investigate the effects of adding cholesterol or another lipid type. In addition, we evaluate the threshold values of the transmembrane potential needed to porate bilayers of various compositions and, in conclusion, summarize these results in terms of lysis tensions.

METHOD DESCRIPTION

Theoretical considerations of pore dynamics

According to Brochard-Wyart et al. (3), the life of a pore in a spherical vesicle of radius R is composed of four consecutive stages. Initially, the pore grows and then stabilizes to its maximal radius. Then, the pore radius decreases slowly in a quasistatic leakout regime, followed by the last stage, fast closure. The pore spends the majority of its lifetime in the third regime, that of slow closure, which we use to determine the edge tension. For a circular pore of radius r , it can be shown (see [Supporting Material](#)) that

$$R^2 \ln(r) = -\frac{2\gamma}{3\pi\eta}t + C, \quad (1)$$

where γ denotes the edge tension, η is the viscosity of the aqueous medium, t is time, and C is a time-independent constant taking one value for each experiment. This equation is obtained by combining three coupled differential equations for the three unknowns R , r , and the vesicle surface tension, σ , using the approximation that r changes slowly (i.e., $r\sigma \approx \gamma$, see [Supporting Material](#)). This final equation is solved assuming constant R .

The principle of the edge-tension measurement is very simple. One only has to consider the linear part of $R^2 \ln(r)$ as a function of time corresponding to the slow closure stage. Linear fit of this part gives a slope, a , and the edge tension, γ , is estimated from the relation $\gamma = -(3/2)\pi\eta a$.

Electromediated pore formation

We trigger the process of electroporation by applying an electric pulse for 5 ms and field strength in the range 20–80 kV/m. The pulse leads to a voltage drop across the membrane of the order of 1 V. Such pulses can create pores several microns in diameter, also referred to as macropores. We monitor the pore size evolution with fast phase-contrast imaging. In this way, we avoid the use of a fluorescent dye or glycerol as in (21) and expect to obtain more accurate values for the edge tension.

Using phase-contrast microscopy, it is possible to accurately measure the size of the pore if it is located in the in-focus area of the vesicle, as has been demonstrated in earlier electroporation and fusion studies (27,28). Here,

the pores were always located in this area and, more precisely, at the vesicle poles facing the electrodes, because of the angular dependence of the transmembrane potential created during the pulse and the chamber geometry (see, e.g., Dimova et al. (29) and Supporting Material). We also employed a conventional trick to improve the contrast in the vesicle images: we used different sugar solutions inside and outside the liposomes. The vesicles were prepared in a sucrose solution and subsequently diluted in a glucose solution. Due to the difference in the refractive indices of these solutions, the vesicles appear as dark objects surrounded by a bright halo on a light gray background (Fig. 1 A). The vesicle membrane is located where the image intensity gradient is maximal. When a pore opens, the two sugar solutions mix and the gradient vanishes in the pore area. Thus, interrupting the membrane continuity in the focal plane, i.e., inducing pores in this area, causes an interruption in the halo, which we used to determine the pore radius. To avoid any bias introduced by manual processing, we developed a program that would automatically measure

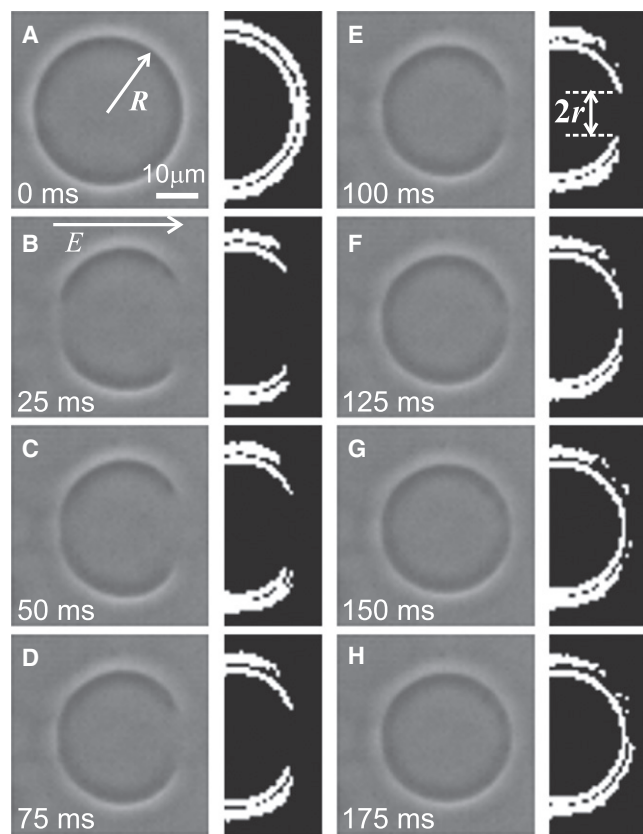


FIGURE 1 Time sequence of raw images (columns 1 and 3) and processed images (columns 2 and 4) of a vesicle with a radius of $17 \mu\text{m}$ exposed to an electric pulse of duration 5 ms and amplitude 50 kV/m. Time $t = 0$ s (A) corresponds to the beginning of the pulse. (B–H) The pore radius r (schematically indicated in E), decreases (B–F), and after ~ 150 ms it has resealed (G and H). The field direction is indicated in B. A pore formed in the left hemisphere of the vesicle is visible in B.

the pore sizes (for details, see Image analysis and Supporting Material).

Let us note that many small suboptical pores located very close to each other could lead to images similar to those obtained for a single big pore. Furthermore, in some cases, several macropores could be created within the same vesicle, occasionally on both sides facing the electrodes. In this case, Eq. 1 is still valid (for justification, see Supporting Material).

The overall vesicle response and behavior of the pores over time as theoretically described in Brochard-Wyart et al. (3) is different from that observed here in the stage of pore formation. The applied electric field leads to a gradual and nonuniform increase of the membrane tension along the vesicle surface. Thus, the theoretical approach in Brochard-Wyart et al. (3), which assumes constant and uniform tension distribution over the entire vesicle, cannot be applied to the period during the pulse. However, after the end of the pulse, the membrane tension is no longer inhomogeneous and the pore closure analysis is applicable (as detailed in Supporting Material).

During the pulse, when the tension exceeds some critical value corresponding to the lysis tension, the membrane ruptures, i.e., a pore is formed. Membrane electroporation is associated with building of some critical transmembrane potential across the bilayer, which we use to evaluate the lysis tension of membranes of various composition.

MATERIALS AND EXPERIMENTAL PROCEDURES

Lipids and solutions

Egg yolk L- α -phosphatidylcholine (eggPC), dioleoylphosphatidylcholine (DOPC), dioleoylphosphatidylethanolamine (DOPE), and L- α -phosphatidyl-ethanolamine-N-(lissamine rhodamine B sulfonyl) (rhodamine-PE) were purchased from Avanti Polar Lipids (Alabaster, AL), and cholesterol was from Sigma (Steinheim, Germany). Four different membrane compositions were studied: DOPC, DOPC/cholesterol at a molar ratio of 5:1, DOPC/DOPE, also at a molar ratio of 5:1, and eggPC fluorescently labeled with rhodamine-PE (1 mol %). Lipids were diluted in chloroform at a mass concentration of 0.5 mg/mL, and stored at -20°C . The vesicles were prepared in an aqueous solution of 240 mM sucrose (internal solution) and subsequently diluted in an aqueous solution of 260 mM glucose and 1 mM sodium chloride (external solution). The pH of the solutions was adjusted to 7 using either 1 mM phosphate buffer ($\text{KH}_2\text{PO}_4/\text{K}_2\text{HPO}_4$, Merck, Darmstadt, Germany) or 1 mM HEPES buffer from Sigma. No difference in the behavior of the vesicles was observed using one buffering agent or the other. The conductivities of the internal and external solutions were measured with a SevenEasy conductivity meter (Mettler Toledo, Greifensee, Switzerland), and had values of $\sim 20 \mu\text{S}/\text{cm}$ and $150 \mu\text{S}/\text{cm}$, respectively. The osmolarities, measured with osmometer Osmomat 030 (Gonotec, Berlin, Germany), were $\sim 260 \text{ mOsm}/\text{kg}$ and $275 \text{ mOsm}/\text{kg}$, respectively.

Giant vesicle preparation

The GUVs were prepared using the electroformation protocol (30) at room temperature, at which all lipids are in the fluid phase. A small volume ($15 \mu\text{L}$) of the lipid solution in chloroform was deposited on the conducting sides of glass slides coated with indium tin oxide. The glasses were then kept for 2 h under vacuum in an oven at 63°C to remove all traces of the organic solvent.

Afterward, the plates, spaced by a 1-mm-thick silicon frame (Electron Microscopy Sciences, Hatfield, PA) were assembled in a chamber. The chamber was filled with the sucrose solution (internal medium). The slides were connected to the AC field function generator Agilent 33220A (Agilent Technology Deutschland, Böblingen, Germany) and sinusoidal voltage of 25 mV peak to peak was applied at 10 Hz. The voltage was increased by 100-mV steps every 5 min to a value of 1225 mV and maintained under these conditions overnight. Shorter times (~2 h) were also sufficient, without altering the results. Finally, the square-wave AC field of the same amplitude was applied at 5 Hz for 1 h to detach the GUVs from the slides.

Application of electric pulses

For pulse application, we used a home-made chamber constructed from a glass slide and a coverslip similar to the one described in Portet et al. (31). Two parallel copper strips (3M, Cergy-Pontoise, France) were stuck on the slide 0.5 cm apart. The coverslip was then glued onto the glass slide with heated parafilm. The cavity between the slide and the coverslip was filled with 30 μ L of the buffered glucose solution and 2 μ L of the GUV solution. Electric pulses of 5 ms duration and amplitudes ranging from 20 to 80 kV/m were applied directly under the microscope with β tech pulse generator GHT_Bi500 (β tech, l'Union, France). The pulse generator was synchronized with the digital camera, so that the image acquisition was triggered by the onset of the pulse.

Microscopy

The GUVs were observed under an inverted microscope (Axiovert 135, Zeiss, Göttingen, Germany) equipped with a 20 \times Ph2 objective. Phase-contrast images were collected at acquisition speeds of 5000, 10,000, or 20,000 frames/s (fps) with a fast digital camera (HG-100K, Redlake, San Diego, CA). Illumination during routine observations was performed with a halogen lamp. A mercury lamp (HBO W/2) was used for image acquisition for a total of a few seconds. During this time, no detectable heating of the sample occurred.

Image analysis

To avoid bias in the pore-size determination, we developed image processing procedures to automatically evaluate the pore radii. The procedure consists of two stages: 1), detection of the vesicle contour, and 2), pore size measurement. We first transformed the raw vesicle image into a binary image, with the membrane represented by the nonzero pixel value. Given such an image, for which the decision of where the membrane was located had already been made, it was then easy to obtain the pore size, r , via custom algorithms (see Supporting Material).

The vesicle radii, R , were measured manually using Image J (National Institutes of Health, Bethesda, MD). As described in the previous section, the linear part of the curve, $R^2 \ln(r)$, as a function of time t was fitted with an expression of the form $y = at + b$, and the edge tension, γ , was obtained from the slope a through $\gamma = -(3/2)\pi\eta a$. For the viscosity of the 260-mM glucose solution, we used $\eta = 1.133 \cdot 10^{-3}$ Pa.s (32). To avoid effects due to change in the vesicle radius, which most often occur before the stage of linear dependence of the data (see Supporting Material), R was measured at the end of this stage.

RESULTS

Edge tension of eggPC membranes

Because the majority of literature data on edge tensions has been collected on eggPC membranes, we first tested our method on GUVs made of this lipid. With fluorescence microscopy of eggPC vesicles labeled with rhodamine-PE (data not shown), we confirmed that single macropores formed on the cathode-facing pole of the vesicles. This supports previous observations on DOPC (33,31) and

indicates that such behavior is not tail-specific but is presumably related to the nature of the lipid headgroup. Only in a limited number of experiments could macropores also be visualized on the anode-facing side of the vesicles. Thus, the pore sizes were measured only at the cathode-facing hemispheres. For the vesicle radii explored here (between 10 and 40 μ m), the applied pulses induce transmembrane potentials of the order of 0.7–1.25 V. The evolution of the closing pore after the end of the pulse could be clearly followed with phase contrast microscopy, as shown in the example in Fig. 1. The very first image shows the unperturbed vesicle.

During the pulse, i.e., in the first 5 ms (data not shown), the vesicles attained a spherocylindrical shape, with symmetry axis along the field direction (see, e.g., Fig. 3 B), as previously reported for GUVs in salt solution (34). The deformation here seemed less pronounced, presumably because of the lower field amplitude used, but appeared to have a longer lifetime, on the order of a few ms as compared to hundreds of μ s in (34), because of the longer pulses applied in this work.

The pores could only be detected after ~5 ms, almost at the end of the pulse. The temporal and optical resolution of our setup did not allow us to detect the pore formation and growth precisely. It appeared that the pore was created already with a rather large radius of a few micrometers, slightly grew in the following few hundreds of microseconds, stabilized in the next couple of milliseconds and then entered the stage of slow closure. This sequence was exhibited by almost every vesicle we studied, for all compositions. It remains unclear whether the poration process was initiated with a single pore created during the pulse, or whether, instead, many smaller pores first formed and then coalesced. If the first scenario is valid, the rate of opening of the macropore should be on the order of several mm/s, i.e., beyond our temporal and spatial resolution. We favor the second hypothesis, with smaller pores of suboptical size, since the critical transmembrane potential for poration is reached already in the beginning of the pulse (see Supporting Material).

We now focus on the stage of pore closure used to determine the edge tension. The images in Fig. 1, B–F, belong to this stage. The pore has completely resealed after 150 ms (see Fig. 1, G and H). The image at 25 ms (Fig. 1 B) shows that the GUV membrane is altered at the anode-facing side as well. This hemisphere has been reported to be the location of smaller pore nucleation (33) and generation of membrane tubes (31), which, apart from the fact that poration was not always observed, was an argument against analyzing the pore closure at this hemisphere. Here, the re-sealing occurred much faster: this side of the liposome is intact on the subsequent pictures. To illustrate the image analysis procedure leading to the quantitative measurement of the pore radius (see also Supporting Material), we present in the second and fourth columns of Fig. 1 the processed

images corresponding to the cathode-facing half of the GUV shown in the adjacent raw images. The outer white circle in the processed image corresponds to the boundary between the bright halo around the vesicle and the gray background, whereas the inner white circle indicates the membrane position. It is this inner circle that is used for pore size measurements. The pore diameter is schematically indicated in Fig. 1 E.

The electroporated GUVs generally decreased in size upon the application of the pulse (as exemplified by the vesicle in Fig. 1). This behavior is consistent with previous reports (31), but questions the assumption of constant R , which was used to derive Eq. 1. However, the change in the vesicle radius, probably linked to the expulsion of small vesicles or the pulling of membrane tubes (31), occurs predominantly in the first hundreds of microseconds after the pulse, followed by a negligible decrease of $\sim 1.5\%$ during the stage of pore closure (see Supporting Material). The latter change is on the order of the error in measuring the pore radius. Thus, our assumption of constant vesicle size in the linear stage of slow pore closure is justified. For the value of R in the fits according to Eq. 1, we used the liposome radius after the pore has closed.

From the images, we extract the time dependence of the pore size. We plot the size of the porated regions characterized by $R^2 \ln(r)$ as a function of time. In Fig. 2, we show six typical datasets from the 41 measurements performed on eggPC GUVs. The linearity of the time dependence of the quantity $R^2 \ln(r)$ in the quasistatic leakout regime and the similar slopes in the different datasets emphasize the validity of the theoretical model. The straight solid lines are fits according to Eq. 1. The edge tension, γ , is deduced from

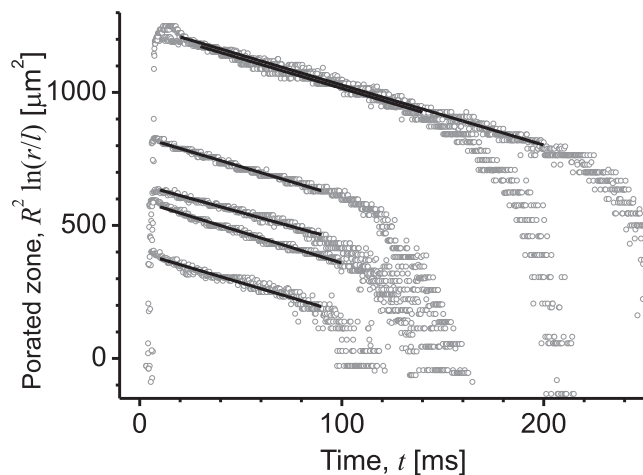


FIGURE 2 Evolution of the porated region as characterized by $R^2 \ln(r/l)$ as a function of time t for six different eggPC vesicles. To avoid plotting a dimensional value in the logarithmic term, we have introduced $l = 1 \mu\text{m}$ (note that this operation does not influence the slope of the curves). The gray open circles are experimental data and the solid lines are linear fits whose slopes yield the edge tension, γ . The vesicle radii, R , are (lower to upper) $12.7 \mu\text{m}$, $16.0 \mu\text{m}$, $17.6 \mu\text{m}$, $21.1 \mu\text{m}$, $20.7 \mu\text{m}$, and $21.7 \mu\text{m}$.

the slopes of these lines. The slopes are similar, because the explored vesicles have identical compositions, i.e., identical edge tension. For eggPC membranes, we found that the mean value of the edge tension was 14.2 pN , with a standard error of 0.7 pN (for other literature data on eggPC, see Table 1).

Each studied vesicle was permeabilized, which led to partial sugar mixing. If the associated loss of optical contrast was not significant, we used the same vesicle a few more times to perform edge tension measurements on the same vesicle and test for reproducibility. In this case, the pulses were well separated in time, e.g., by an interval of $\sim 5 \text{ min}$. A total of 41 experiments were carried out on 16 GUVs from different preparations.

Effect of membrane composition

Having tested our approach on eggPC and achieved significantly better accuracy than with other methods, we proceeded to examine membranes of different compositions. We first tested vesicles made of DOPC because 1), this lipid has been used in other studies (15,21,35), which could provide a basis for comparison with our results; and 2), DOPC is a pure lipid type, as compared with eggPC, which is composed of several lipid species that may influence the measured edge tensions.

The edge tensions for DOPC membranes obtained from electroporation of black lipid membranes (15), light-induced poration of GUVs (21), or AFM studies on supported bilayers (35) range from 3.9 to 25 pN (Table 1). The upper value corresponds to DOPC purchased from the same producer as ours (Avanti Polar Lipids); for details on effects of lipids from different producers, see Karatekin et al. (21). Applied to DOPC GUVs, our method yielded $\gamma = 27.7 \pm 2.5 \text{ pN}$ for the edge tension from a total of 24 experiments. This value is comparable to previous results.

After characterizing the edge tension of pure DOPC membranes, we proceeded to examine differences resulting from the presence of small fractions of guest molecules in the membrane. We considered the effect of cholesterol because it is ubiquitous in eukaryotic membranes. The inverted-cone shape of this molecule should prevent it from locating at the rim of the pore. Thus, the presence of cholesterol would require more energy to rearrange the lipids along the pore walls, and the edge tension is expected to increase (21). Indeed, for membranes made of DOPC/cholesterol at a 5:1 molar ratio, we found an edge-tension value of $36.4 \pm 1.9 \text{ pN}$ (mean \pm SE) from a total of 14 experiments, confirming our expectations and a trend reported previously (21).

Similar to the experiments with cholesterol, we probed the effect of DOPE, which to our knowledge has not been explored. Like cholesterol, this lipid has an inverted-cone shape and is thus expected to lead to an increase in the edge tension (21). However, membranes with the same molar

TABLE 1 Edge tensions and poration thresholds for different membrane compositions

Membrane composition	Edge tension, γ (pN)	Method	Poration threshold, $\Delta\psi_c$ (mV)	Lysis tension, σ_{lys} (mN/m)	Reference
EggPC	14.2 ± 0.7 [41]	Pore closure dynamics and electroporation	920 ± 20	3.79	This work
EggPC	20	Observation of open cylindrical vesicles			(18)
EggPC	8.6 ± 0.4	Electroporation of black lipid membranes			(52)
EggPC	42	Observation of the disk-vesicle transition			(4)
EggPC	8.6 ± 0.4	Electroporation of black lipid membranes			(14)
EggPC	21	Electroporation of black lipid membranes			(15)
DOPC	27.7 ± 2.5 [24]	Pore closure dynamics and electroporation	950 ± 30	4.08	This work
DOPC	25	Electroporation of black lipid membranes			(15)
DOPC from Avanti	20.7 ± 3.5	Pore closure dynamics and light-induced poration			(21)
DOPC from Sigma	6.9 ± 0.42	Pore closure dynamics and light-induced poration			(21)
DOPC	13–18	Pore closure dynamics and light-induced poration			(40)
DOPC	3.9 ± 0.3	Atomic force microscopy			(35)
DOPC/cholesterol 5:1 (mol)	36.4 ± 1.9 [14]	Pore closure dynamics and electroporation	680 ± 20	1.89	This work
DOPC/cholesterol mixtures	9–22	Pore closure dynamics and light-induced poration			(21)
SOPC	9.2 ± 0.7	Micropipette aspiration and electroporation	1100	4.91	(19,42)
SOPC/cholesterol 1:1 (mol)	30.5 ± 1.2	Micropipette aspiration and electroporation	1800		(19,42)
SOPC/cholesterol 1:1 (mol)	26	Reinterpretation of results from Zhelev and Needham (19)			(56)
DOPC:DOPE 5:1 (mol)	15.6 ± 1.3 [31]	Pore closure dynamics and electroporation	880 ± 40		This work
EggPE	15 ± 1	Electroporation of black lipid membranes			(14)
<i>Escherichia coli</i> PE	16 ± 0.6	Electroporation of black lipid membranes			(52)
DOPC/Tween 20 mixtures	0.2–12	Pore closure dynamics and light-induced poration			(21,40)

Edge tensions for different membrane compositions measured here and by other groups. The standard errors are given, unless otherwise indicated, in the respective literature reference. Numbers in square brackets indicate the measurements performed for each composition. Data on the critical transmembrane potential and estimates for lysis tension (see Supporting Material) are also given.

fraction of the guest molecules, i.e., DOPC/DOPE at a 5:1 molar ratio, yielded quite an unexpected result. We found a significant decrease of the edge tension compared to pure DOPC, with a value of 15.6 ± 1.3 pN estimated from 31 experiments.

All our results are summarized in Table 1, including edge tensions obtained by other groups.

Electroporation thresholds and stability of membranes of various compositions

Although eggPC, DOPC, and DOPC/DOPE GUVs exposed to electric pulses of a few tens of kV/m porated and resealed very quickly, DOPC/cholesterol vesicles exposed to such field amplitudes were completely destabilized. The GUVs burst and disintegrated in a fashion reminiscent of the behavior observed with charged membranes (36). An image sequence of such an event is given in Fig. 3. To avoid vesicle destruction, we applied pulses with lower amplitudes for the

edge tension measurements, around half the strength used for the other membrane compositions. At these reduced amplitudes, DOPC/cholesterol vesicles porated and resealed in the usual manner. Note that such weak pulses did not porate the cholesterol-free vesicles. This indicates that cholesterol lowers the stability of DOPC membranes when exposed to electric pulses.

As a characteristic of membrane stability in electric fields, one can consider the critical transmembrane potential, $\Delta\psi_c$, at which poration occurs. Following the approach of Schwan, see first chapter in Ref. (37), at the moment of maximally expanded pore, we define the critical transmembrane potential as $\Delta\psi_c = (3/2)R_{in}E\cos(\theta_p)$, where R_{in} denotes the initial vesicle radius before poration, E is the field magnitude, and θ_p is the inclination angle defining the location of the pore edge with respect to the vesicle center (see Supporting Material). This expression can be presented as $\Delta\psi_c = (3/2)E\sqrt{R_{in}^2 - r_m^2}$, where r_m is the maximal pore size. Thus, measuring r_m after applying

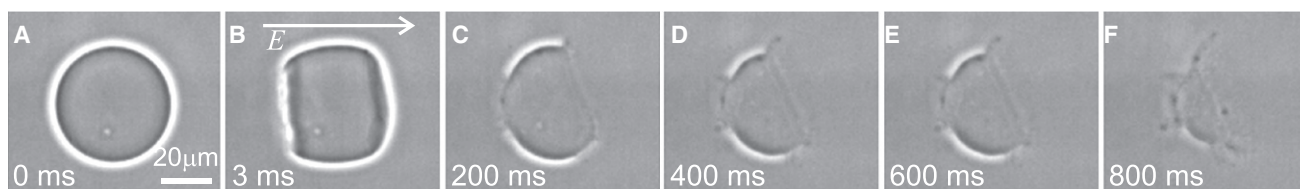


FIGURE 3 Image sequence of a collapsing vesicle made of DOPC:cholesterol 5:1 exposed to a pulse with a field strength of 50 kV/m and a duration of 5 ms. The field direction is indicated in B, where the vesicle attains a spherocylindrical shape.

a pulse with field strength E provides us with an estimate for the critical transmembrane potential, $\Delta\psi_c$. The results for the four mixtures explored are included in [Table 1](#). Although the cholesterol-free membranes porate at similar values of $\Delta\psi_c$, ~ 0.9 V, the addition of 17 mol % cholesterol to DOPC bilayers (DOPC/cholesterol 5:1) decreases the critical transmembrane potential to ~ 0.7 V, i.e., destabilizes these membranes when exposed to an electric pulse.

As mentioned in the section Electromediated pore formation, the critical transmembrane potential is related to the so-called lysis tension, σ_{lys} . The latter can be deduced (see [Table 1](#)) given available knowledge about the membrane thickness (for details, see [Supporting Material](#)). From the decrease in the critical transmembrane potential we find that cholesterol lowers the lysis tension of DOPC membranes.

DISCUSSION

In this section, we emphasize some advantages of our approach and then compare the edge tension data measured here with previously reported results obtained by other methods. First, our approach is relatively easy to apply in a moderately equipped lab. The experiments can be performed using a simple home-made chamber with two electrodes and a microscope. Even though we used a fast digital camera for the acquisition of images, we did not exploit the full potential of this equipment. Indeed, conventional cameras with an acquisition speed of ~ 1000 fps are now reasonably priced and widely available on the market. Such an acquisition speed is more than sufficient for collecting a reasonable amount of data in the time range of interest between 5 and 100 ms (see [Fig. 2](#)). Second, the total measuring time is < 5 min. This allows us to perform a significant number of measurements and achieve good data statistics. Note that studies in the literature that report measurements on giant vesicles very often base their findings on not more than five experiments (for example, the method reported in Harbich and Helfrich (18) was applied to three vesicles only). Most often, the number of measurements is not even mentioned. Achieving good data statistics is important, particularly when multicomponent membranes are examined. For example, in vesicles prepared from DOPC, sphingomyelin, and cholesterol, Veatch and Keller (38) have estimated a variation of 2 mol % cholesterol between individual vesicles prepared by the electroformation method. Inspection of fluorescent images of DOPC, dioleoylphosphatidylglycerol, and cholesterol, which have undergone phase separation, suggests that this spread may be even larger for certain compositions (39). For this reason, when dealing with multicomponent vesicles one should examine large populations of liposomes. The increase in research activity on more complex membrane compositions accentuates the need to develop methods that can quickly and easily be applied to many vesicles. Our method fulfills this requirement. Third, compared to other methods, our

approach is of high precision and makes it possible to measure the edge tension with a relatively small error. Finally, in contrast to certain other procedures (21,40), our experimental approach does not require the presence of 1), a very viscous solvent (typically 66 vol % glycerol) to slow down the pore closure dynamics, or 2), fluorescent dye to visualize the pore. As discussed above, both of these compounds may influence the edge-tension value.

We measured the edge tension of membranes of various compositions, and found it to be 27.7 and 14.2 pN for pure DOPC and eggPC bilayers, respectively. Considering the multicomponent character of eggPC, this result is understandable: small fractions of edge active lipid molecules in eggPC can stabilize the pore and lower the edge energy compared to pores in pure DOPC bilayers. Our literature survey shows a significant scatter of the data for eggPC. Values of γ were reported to range from 8.6 to 42 pN (see [Table 1](#)). We presume that eggPC purchased from different producers can vary in terms of composition. Impurities in synthetic lipids like DOPC can also lead to significant variation, as demonstrated in Karatekin et al. (21). Indeed, our results for DOPC are closer to the upper value reported in the Karatekin study (21) and to the value measured by Genco et al. (15), which is to be expected keeping in mind that our lipid was purchased from the same producer (see [Table 1](#), *second column*). This finding contradicts results obtained using a method in which supported lipid bilayers are punctured by means of an AFM cantilever tip (13). This latter method seems to give systematically lower values for edge tension (see [Table 1](#) for data on DOPC (35) and palmitoyl-oleoylphosphatidylcholine (POPC) (41)). We can only speculate that the presence of the substrate supporting the bilayer might influence the pore stability and thus the edge tension. We presume that this method is still applicable when examining relative changes in the edge tension resulting from the presence of edge active molecules (41) or in lipid mixtures (35).

The inclusion of cholesterol in DOPC membranes (5:1 mol/mol or ~ 17 mol %) led to two interesting observations, destabilization of the membrane upon exposure to electric pulses and an increase in edge tension, which we discuss next.

Electric pulses of 5-ms duration, which induce transmembrane voltages of ~ 1.25 V, lead to irreversible collapse of cholesterol-containing liposomes ([Fig. 3](#)). Reversible poration of these liposomes required the application of pulses with about half the field strength, i.e., transmembrane voltages of ~ 0.7 V. Such pulses did not appear to cause poration in other membrane types, but were able to successfully porate the DOPC/cholesterol GUVs. As shown in [Table 1](#), the critical transmembrane potential needed to rupture the DOPC membrane is lowered by the presence of cholesterol. This observation is interesting and unexpected given the somewhat opposite effect of cholesterol observed on stearoyl-oleoylphosphatidylcholine (SOPC)

giant vesicles (19,42). In SOPC membranes, cholesterol was found to increase the critical poration threshold $\Delta\psi_c$ (see Table 1). On the other hand, dipalmitoylphosphatidylcholine vesicles doped with 12 and 20 mol % of cholesterol appear to porate at transmembrane potentials lower than that of pure dipalmitoylphosphatidylcholine membranes (43). Finally, for eggPC planar membranes (15) and vesicles (43) no effect of cholesterol on the critical permeabilization potential was observed. In summary, cholesterol, which alters the hydrophobic core of the bilayer, affects the membrane stability differently depending on the molecular architecture of the lipid building the membrane.

Recent studies suggest that the effect of cholesterol on another material property of membranes, namely, the bending stiffness, is also lipid-specific and depends on the degree of unsaturation of the acyl chains (44–46). Earlier conventional beliefs held that by ordering the acyl chains in fluid membranes, cholesterol inherently leads to an increase in their bending rigidity. This concept was supported by observations on lipids such as SOPC (47,48), dimyristoylphosphatidylcholine (49,50), and POPC (51). However, as demonstrated recently (44,46), the bending rigidity of DOPC/cholesterol mixtures does not show any significant correlation with the cholesterol content, whereas in sphingomyelin/cholesterol membranes it even decreased (46). The origin of the cholesterol-induced lowering of the critical poration potential in DOPC membranes may be found in its effect of decreasing the membrane conductivity, justified in detail in Raffy and Teissié (43). This behavior may be related to lipid ordering. Our results suggest that the influence of cholesterol on the mechanical properties of lipid membranes depends on the specific lipid architecture and is far from being fully elucidated. Further studies of the influence of cholesterol on the membrane properties as a function of lipid type and cholesterol content have still to be performed. Here, we emphasize only that the critical transmembrane potential of such membranes is a physical parameter very sensitive to membrane composition and can be employed to characterize various types of membranes and the effect of cholesterol as shown by our data.

Although DOPC membranes appear to be destabilized by the addition of cholesterol, as illustrated by a decrease in the critical transmembrane potential and the lysis tension, the edge tension is observed to increase from 27.7 pN for pure DOPC to 36.4 pN for vesicles made of DOPC/cholesterol 5:1. This is consistent with the trend reported in Karatekin et al. (21), where the dependence of the edge tension, γ , as a function of the cholesterol molar fraction, x , was empirically extracted to be $\gamma = \gamma_0 + 26.7x$, where γ_0 is the edge tension of the cholesterol-free bilayer. This expression predicts slightly lower edge tension both for the DOPC membranes measured here and for the SOPC vesicles studied previously (19) (for exact values, see Table 1). The effect of cholesterol increasing the edge tension is expected, considering the inverted-cone shape

of the molecule that is supposed to penalize lipid rearrangement at the pore edge (21).

To summarize, pore stability in DOPC membranes is less favored in the presence of cholesterol. The larger value of γ makes pores close faster. On the other hand, cholesterol reduces the lysis tension by inducing structural changes in the bilayer. This is corroborated by our observation that weaker pulses, which do not have any significant effect on cholesterol-free vesicles, were sufficient to porate the DOPC/cholesterol liposomes.

We also studied the edge-tension effect of another lipid molecule, DOPE, in DOPC GUVs at the same fraction of ~17 mol %. Compared to pure DOPC membranes, we found a significant decrease in the edge tension, from 27.7 to 15.6 pN upon addition of DOPE, reminiscent of effects induced by surfactants (21,40) (see γ value for DOPC mixtures with the detergent Tween 20 in Table 1). It is interesting to note that γ values similar to those obtained for DOPC/DOPE 5:1 were observed for eggPE and PE extracts from *Escherichia coli* (14,52). Within the framework of the membrane elasticity theory, and considering the inverted-cone shape of the DOPE molecule, one would expect an increase in the edge tension upon DOPE addition, analogous to the effect of cholesterol (21). Our results contradict this view. We presume that the molecular architecture of PE lipids that leads to the tendency to form an inverted hexagonal phase, which facilitates fusion and vesicle leakage (see, e.g., Ellens et al. (53)), is also responsible for stabilizing pores and lowering the edge tension in porated membranes, as demonstrated here. A plausible explanation for this behavior is also provided by the propensity of PE to form interlipid hydrogen bonds (54,55). This behavior is not observed for pure PC bilayers, where the edge tension is higher. Our observations suggest that simplistic pictures based on the inverted-cone shape of DOPE are not realistic for the interpretation of pore behavior and edge tensions. Inter-PE hydrogen bonding in the pore region can effectively stabilize pores. It would be interesting to test this hypothesis with simulation studies.

CONCLUSIONS

We have successfully developed and applied a new, to our knowledge, method for edge-tension measurements on GUVs. This method is based on the theoretical model introduced in Brochard-Wyart et al. (3) and relies on the study of pore closure dynamics. Combining membrane electroporation, fast phase-contrast imaging and digital-image analysis, we were able to monitor the rate of pore closure and deduce the edge tension of membranes with different compositions. This method is fast and quite easy to apply, and we believe it could be of use to researchers interested in the mechanical properties of biological membranes. Our results confirm those of studies reporting the tendency of cholesterol to increase the edge tension of lipid membranes. However,

cholesterol appears to have an unconventional and lipid-specific effect on the membrane stability in electric fields, as reflected by the values measured for the critical transmembrane potential and lysis tension. Contrary to our expectations, the addition of DOPE in DOPC vesicles leads to a decrease in the edge tension, which is not, even qualitatively, predicted by current understanding in the field. We hope our results will provoke some theoretical work in this direction.

SUPPORTING MATERIAL

Text and one figure are available at [http://www.biophysj.org/biophysj/supplemental/S0006-3495\(10\)01179-3](http://www.biophysj.org/biophysj/supplemental/S0006-3495(10)01179-3).

We thank J. Teissié for his assistance in purchasing the β tech pulse generator, and M.-P. Rols and D. S. Dean for critical reading of the manuscript. T.P.'s stay in Germany was supported by a grant for international mobility of Ph.D. students from the Université de Toulouse. We acknowledge financial support from the Association Française contre les Myopathies.

REFERENCES

- Litster, J. D. 1975. Stability of lipid bilayers and red blood cell membranes. *Phys. Lett.* 53A:193–194.
- Boal, D. 2002. *Mechanics of the Cell*. Cambridge University Press, New York.
- Brochard-Wyart, F., P. de Gennes, and O. Sandre. 2000. Transient pores in stretched vesicles: role of leak-out. *Physica A*. 278:32–51.
- Fromherz, P., C. Röcker, and D. Ruppel. 1986. From discoid micelles to spherical vesicles; the concept of edge activity. *Faraday Discuss.* 81:39–48.
- Newman, C. M. H., and T. Bettinger. 2007. Gene therapy progress and prospects: ultrasound for gene transfer. *Gene Ther.* 14:465–475.
- Escoffre, J.-M., T. Portet, ..., M. P. Rols. 2009. What is (still not) known of the mechanism by which electroporation mediates gene transfer and expression in cells and tissues. *Mol. Biotechnol.* 41: 286–295.
- Leontiadou, H., A. E. Mark, and S. J. Marrink. 2004. Molecular dynamics simulations of hydrophilic pores in lipid bilayers. *Biophys. J.* 86:2156–2164.
- Jiang, F. Y., Y. Bouret, and J. T. Kindt. 2004. Molecular dynamics simulations of the lipid bilayer edge. *Biophys. J.* 87:182–192.
- Tolpekina, T. V., W. K. den Otter, and W. J. Briels. 2004. Simulations of stable pores in membranes: system size dependence and line tension. *J. Chem. Phys.* 121:8014–8020.
- Taupin, C., M. Dvolaitzky, and C. Sauterey. 1975. Osmotic pressure induced pores in phospholipid vesicles. *Biochemistry*. 14:4771–4775.
- Pabst, G., A. Hodzic, ..., P. Laggner. 2007. Rigidification of neutral lipid bilayers in the presence of salts. *Biophys. J.* 93:2688–2696.
- Chang, D. C., and T. S. Reese. 1990. Changes in membrane structure induced by electroporation as revealed by rapid-freezing electron microscopy. *Biophys. J.* 58:1–12.
- Loi, S., G. Sun, ..., H. J. Butt. 2002. Rupture of molecular thin films observed in atomic force microscopy. II. Experiment. *Phys. Rev. E Stat. Nonlin. Soft Matter Phys.* 66:031602.
- Melikyan, G. B., N. S. Matinyan, and V. B. Arakelian. 1990. The influence of gangliosides on the hydrophilic pore edge line tension and monolayer fusion of lipid membranes. *Biochim. Biophys. Acta.* 1030:11–15.
- Genco, I., A. Gliozzi, ..., E. Scalas. 1993. Electroporation in symmetric and asymmetric membranes. *Biochim. Biophys. Acta.* 1149:10–18.
- Luisi, P., and P. Walde. 2000. *Giant Vesicles. Perspectives in Supramolecular Chemistry.*, vol. 6. Wiley & Sons, Chichester, United Kingdom.
- Dimova, R., S. Aranda, ..., R. Lipowsky. 2006. A practical guide to giant vesicles. Probing the membrane nanoregime via optical microscopy. *J. Phys. Condens. Matter.* 18:S1151–S1176.
- Harbich, W., and W. Helfrich. 1979. Alignment and opening of giant lecithin vesicles by electric fields. *Z. Naturforsch. C.* 34a:1063–1065.
- Zhelev, D. V., and D. Needham. 1993. Tension-stabilized pores in giant vesicles: determination of pore size and pore line tension. *Biochim. Biophys. Acta.* 1147:89–104.
- Sandre, O., L. Moreaux, and F. Brochard-Wyart. 1999. Dynamics of transient pores in stretched vesicles. *Proc. Natl. Acad. Sci. USA.* 96:10591–10596.
- Karatekin, E., O. Sandre, ..., F. Brochard-Wyart. 2003. Cascades of transient pores in giant vesicles: line tension and transport. *Biophys. J.* 84:1734–1749.
- Reference deleted in proof.
- Westh, P. 2003. Unilamellar DMPC vesicles in aqueous glycerol: preferential interactions and thermochemistry. *Biophys. J.* 84:341–349.
- May, S. 2000. A molecular model for the line tension of lipid membranes. *Eur. Phys. J. E.* 3:37–44.
- Ayuyan, A. G., and F. S. Cohen. 2006. Lipid peroxides promote large rafts: effects of excitation of probes in fluorescence microscopy and electrochemical reactions during vesicle formation. *Biophys. J.* 91:2172–2183.
- Zhao, J., J. Wu, ..., G. Feigenson. 2007. Phase studies of model biomembranes: macroscopic coexistence of $L\alpha + L\beta$, with light-induced coexistence of $L\alpha + L_0$ phases. *Biochim. Biophys. Acta.* 1768:2777–2786.
- Riske, K. A., and R. Dimova. 2005. Electro-deformation and poration of giant vesicles viewed with high temporal resolution. *Biophys. J.* 88:1143–1155.
- Haluska, C. K., K. A. Riske, ..., R. Dimova. 2006. Time scales of membrane fusion revealed by direct imaging of vesicle fusion with high temporal resolution. *Proc. Natl. Acad. Sci. USA.* 103: 15841–15846.
- Dimova, R., K. A. Riske, ..., R. Lipowsky. 2007. Giant vesicles in electric fields. *Soft Matter.* 3:817–827.
- Angelova, M. I., and D. S. Dimitrov. 1986. Liposome electroformation. *Faraday Discuss.* 81:303–311.
- Portet, T., F. Camps i Febrer, ..., D. S. Dean. 2009. Visualization of membrane loss during the shrinkage of giant vesicles under electroporation. *Biophys. J.* 96:4109–4121.
- Weast, R. 1988. *Handbook of Chemistry and Physics*. CRC Press, Boca Raton, FL.
- Tekle, E., R. D. Astumian, ..., P. B. Chock. 2001. Asymmetric pore distribution and loss of membrane lipid in electroporated DOPC vesicles. *Biophys. J.* 81:960–968.
- Riske, K. A., and R. Dimova. 2006. Electric pulses induce cylindrical deformations on giant vesicles in salt solutions. *Biophys. J.* 91: 1778–1786.
- Chiantia, S., J. Ries, ..., P. Schwille. 2006. Combined AFM and two-focus SFCS study of raft-exhibiting model membranes. *ChemPhysChem.* 7:2409–2418.
- Riske, K., R. Knorr, and R. Dimova. 2009. Bursting of charged multicomponent vesicles subjected to electric pulses. *Soft Matter.* 5:1983–1986.
- Neumann, E., A. E. Sowers, and C. A. Jordan. 1989. *Electroporation and Electrofusion in Cell Biology*. Plenum, New York.
- Veatch, S. L., and S. L. Keller. 2003. A closer look at the canonical ‘raft mixture’ in model membrane studies. *Biophys. J.* 84:725–726.
- Vequi-Suplicy, C. C., K. A. Riske, ..., R. Dimova. 2010. Vesicles with charged domains. *Biochim. Biophys. Acta.* 1798:1338–1347.

40. Puech, P.-H., N. Borghi, ..., F. Brochard-Wyart. 2003. Line thermodynamics: adsorption at a membrane edge. *Phys. Rev. Lett.* 90:128304.
41. García-Sáez, A. J., S. Chiantia, ..., P. Schwille. 2007. Pore formation by a Bax-derived peptide: effect on the line tension of the membrane probed by AFM. *Biophys. J.* 93:103–112.
42. Needham, D., and R. M. Hochmuth. 1989. Electro-mechanical permeabilization of lipid vesicles. Role of membrane tension and compressibility. *Biophys. J.* 55:1001–1009.
43. Raffy, S., and J. Teissié. 1999. Control of lipid membrane stability by cholesterol content. *Biophys. J.* 76:2072–2080.
44. Pan, J. J., T. T. Mills, ..., J. F. Nagle. 2008. Cholesterol perturbs lipid bilayers nonuniversally. *Phys. Rev. Lett.* 100:198103.
45. Pan, J., S. Tristram-Nagle, ..., J. F. Nagle. 2008. Temperature dependence of structure, bending rigidity, and bilayer interactions of dioleoylphosphatidylcholine bilayers. *Biophys. J.* 94:117–124.
46. Gracia, R. S., N. Bezlyepkina, ..., R. Dimova. 2010. Effect of cholesterol on the rigidity of saturated and unsaturated membranes: fluctuation and electrodeformation analysis of giant vesicles. *Soft Matter* 6:1472–1482.
47. Evans, E., and W. Rawicz. 1990. Entropy-driven tension and bending elasticity in condensed-fluid membranes. *Phys. Rev. Lett.* 64:2094–2097.
48. Song, J. B., and R. E. Waugh. 1993. Bending rigidity of SOPC membranes containing cholesterol. *Biophys. J.* 64:1967–1970.
49. Duwe, H. P., J. Kaes, and E. Sackmann. 1990. Bending elastic moduli of lipid bilayers: modulation by solutes. *J. Phys. IV.* 51:945–962.
50. Méléard, P., C. Gerbeaud, ..., P. Bothorel. 1997. Bending elasticities of model membranes: influences of temperature and sterol content. *Biophys. J.* 72:2616–2629.
51. Henriksen, J., A. C. Rowat, ..., J. H. Ipsen. 2006. Universal behavior of membranes with sterols. *Biophys. J.* 90:1639–1649.
52. Chernomordik, L., M. Kozlov, ..., Y. Chizmadzhev. 1985. The shape of lipid molecules and monolayer membrane fusion. *Biochim. Biophys. Acta.* 812:641–655.
53. Ellens, H., J. Bentz, and F. C. Szoka. 1986. Fusion of phosphatidylethanolamine-containing liposomes and mechanism of the L α -HII phase transition. *Biochemistry.* 25:4141–4147.
54. Lewis, R. N. A. H., and R. N. McElhaney. 1993. Calorimetric and spectroscopic studies of the polymorphic phase behavior of a homologous series of n-saturated 1,2-diacyl phosphatidylethanolamines. *Biophys. J.* 64:1081–1096.
55. Pink, D. A., S. McNeil, ..., M. J. Zuckermann. 1998. A model of hydrogen bond formation in phosphatidylethanolamine bilayers. *Biochim. Biophys. Acta.* 1368:289–305.
56. Moroz, J. D., and P. Nelson. 1997. Dynamically stabilized pores in bilayer membranes. *Biophys. J.* 72:2211–2216.

Biophysical Journal, Volume 99

Supporting Material

A New Method for Measuring Edge Tensions and Stability of Lipid Bilayers: Effect of Membrane Composition

Thomas Portet and Rumiana Dimova

A New Method for Measuring Edge Tensions
and Stability of Lipid Bilayers:
Effect of Membrane Composition
(Supporting Material)

Thomas Portet

Institut de Pharmacologie et de Biologie Structurale,
CNRS UMR 5089, Université Paul Sabatier, Toulouse, France
and

Laboratoire de Physique Théorique,
CNRS UMR 5152, Université Paul Sabatier, Toulouse, France.

Rumiana Dimova ¹

Max Planck Institute of Colloids and Interfaces,
Potsdam, Germany.

November 1, 2010

¹Corresponding author. Address: Max Planck Institute of Colloids and Interfaces, Science Park Golm, 14424 Potsdam, Germany. Tel.: +49 331 567 9615, Fax: +49 331 567 9612, E-mail: Rumiana.Dimova@mpikg.mpg.de

1 Theoretical considerations of pore dynamics

The description below follows the theoretical model introduced in (1). We consider a spherical vesicle of initial radius R_{in} under tension σ_0 , embedded in a medium of bulk viscosity η . When the tension of the vesicle increases, a pore can be created, which relaxes the tension. Thus, we have three dynamic variables possibly coupled to each other: the current vesicle radius R , the membrane tension σ , and the pore radius r . A set of three equations can fully describe the system evolution. Considering the stretching of the membrane by the tension σ and assuming that the total amount of lipid in the vesicle is conserved during the opening and closing of the pore, from the pore and vesicle areas we obtain:

$$\frac{\sigma}{\sigma_0} = 1 - \frac{r^2}{r_c^2} - \frac{4(R_{in}^2 - R^2)}{r_c^2}, \quad (1)$$

where $r_c^2 = 4(R_{in}^2 - R_0^2)$, and R_0 denotes the radius of the vesicle under zero tension. The second equation is given by pore dynamics in vesicles and reads (1):

$$\eta_S \frac{\dot{r}}{r} = \sigma - \frac{\gamma}{r}, \quad (2)$$

where η_S denotes the surface viscosity of the lipid membrane (note that it is related to the membrane 'bulk' viscosity η_m via $\eta_S = d\eta_m$ where d is the membrane thickness), γ is the edge tension, and \dot{r} is the derivative of r with respect to time t . The third and last equation governing the vesicle radius R is derived considering the flux of internal solution through the pore and estimating the leakout velocity by equating the Laplace pressure and the shear stresses involved. It reads

$$\frac{2\sigma}{3\eta R} r^3 = -4\pi R^2 \dot{R}, \quad (3)$$

η being the bulk viscosity of the surrounding medium. We now dispose of a set of three equations governing the evolution of the three variables r , R and σ . Brochard-Wyart et al. carried out a detailed numerical study of this system of equations, providing analytical solutions for some limiting cases (1). Here, we focus on the results for the limit corresponding to our experiments. In this limit, there are four consecutive stages in the pore life: (i) a growth period; (ii) reaching of the maximal pore radius; (iii) a quasi-static leakout regime during which r decreases slowly; and (iv) the last stage of fast closure. These two later stages can be distinguished in the data shown in Fig. 2 in the main text. The pore spends the majority of its

lifetime in the third regime of slow closure, which we use to determine the edge tension. If the pore radius changes very slowly, we can make the quasi-static approximation $r\sigma \approx \gamma$ from Eq. 2. This approximation is reasonable if we evaluate the left-hand-side (LHS) term in Eq. 2. The surface viscosity of the membrane η_S is on the order of 5×10^{-9} Ns/m (2). The rate of pore closing \dot{r} is approximately 5×10^{-5} m/s as seen from our experiments: a pore of radius $r = 5 \mu\text{m}$ closes within about 100 ms. Thus, the LHS term in Eq. 2 is on the order of 5×10^{-8} N/m. The term γ/r on the right-hand side of the equation is at least on the order of $10 \text{ pN}/5 \mu\text{m}$, i.e., 2×10^{-6} N/m. The LHS term is negligible compared to this term, which justifies the assumption that r changes slowly. The membrane tension is also not expected to vary significantly as long as the pore is present in the vesicle. We differentiate Eq. 1 with respect to time to obtain

$$r\dot{r} \approx 4R\dot{R} . \quad (4)$$

Inserting Eq. 4 and $r\sigma \approx \gamma$ into Eq. 3 finally yields

$$R^2 \frac{\dot{r}}{r} \approx -\frac{2\gamma}{3\pi\eta} . \quad (5)$$

If we integrate this equation assuming R stays constant (in section 5 we justify this assumption), we find that the quantity $R^2 \ln(r)$ should decrease linearly as a function of time t with a slope $a = -2\gamma/(3\pi\eta)$. We monitor the evolution of the pore radius r and measure the vesicle radius R . From the linear part of $R^2 \ln(r)$ corresponding to the slow closure stage we extract the slope a . The edge tension γ is then obtained from the relation $\gamma = -(3/2)\pi\eta a$.

2 Transmembrane potential and lysis tension

Lipid bilayers are impermeable to ions. In the presence of an electric field, charges accumulate at the bilayer interface building the transmembrane potential, $\Delta\psi$, across the membrane. At time t , the potential induced on a nonconductive membrane by a DC pulse is given by (3):

$$\Delta\psi(t, \theta) = \frac{3}{2}R |\cos(\theta)| E \left[1 - \exp\left(-\frac{t}{\tau_c}\right) \right] , \quad (6)$$

where R is the vesicle radius, E is the magnitude of the applied field, θ is the angle between the vesicle surface normal and the direction of the electric field, and τ_c is the membrane charging time, given by (3):

$$\tau_c = RC_m \left(\frac{1}{\lambda_{in}} + \frac{1}{2\lambda_{ex}} \right). \quad (7)$$

Here, C_m is the membrane capacitance, $C_m \approx 1 \mu\text{F}/\text{cm}^2$ for lipid membranes (4), and λ_{in} and λ_{ex} are the conductivities of the solutions in the vesicle interior and exterior, respectively. For our experiments in solutions with low conductivity and for explored vesicle radii in the range 10-40 μm , τ_c lies between 50 μs for small GUVs and 250 μs for the larger ones.

Above some critical transmembrane potential $\Delta\psi_c$, the membrane pores, becoming conductive and permeable. The relatively short charging time of our system implies that the critical transmembrane potential is reached already during the pulse, i.e., poration occurs within the first couple of milliseconds. This supports our hypothesis that the observed macropores originate from coalescence of smaller suboptical pores. At the time of maximally expanded pore, the critical transmembrane potential can be estimated using Eq. 6. Since the charging time (at most 250 μs) is much shorter than the time at which the maximally expanded pore is observed (several milliseconds), the exponential term can be ignored. We evaluate the transmembrane potential in the area around the edge of the pore replacing θ with the angle θ_p delimiting the pore boundaries, see also section Electroporation thresholds and stability of membranes with various compositions in the main text. This is a rather crude approximation, which probably leads to slightly overestimating the critical transmembrane potential $\Delta\psi_c$, but as discussed in the main text, the values obtained with this procedure agree well with data reported in the literature.

The electroporation phenomenon can also be understood in terms of a stress in the bilayer created by the electric field. The transmembrane potential induces an effective electrical tension σ_{el} , as defined by the Maxwell stress tensor (4, 5). This tension is given by

$$\sigma_{el} = \epsilon_m \epsilon_0 \left(\frac{h}{2h_e^2} \right) \Delta\psi^2, \quad (8)$$

where ϵ_m and ϵ_0 are the membrane and vacuum permittivities, respectively, h is the total bilayer thickness and h_e is the dielectric thickness. For vesicles with some initial tension σ_0 , the total tension reached during the pulse is

$$\sigma = \sigma_0 + \sigma_{el}. \quad (9)$$

The total membrane tension cannot exceed the tension of rupture, also known as lysis tension. For lipid membranes, the lysis tension σ_{lys} is on

the order of 5 mN/m (4, 6). Neglecting the initial membrane tension σ_0 (see next paragraph), we evaluated $\sigma_{lys} \cong \sigma_{el}(\Delta\psi_c)$ for different membrane compositions using Eq. 8. The values of the total bilayer thickness, h , were taken from (7, 8). For the values of the dielectric thickness we have taken $h_e = h - 0.99$ nm, which accounts for the PC headgroup region (9). For the membrane permittivity we used $\epsilon_m = 2$, even though $\epsilon_m = 4$ is also reported. If the latter number is taken, the estimates for the lysis tension are twice higher than those given in Table 1. The values of σ_{lys} exhibit the same trends as the critical poration potentials.

Lipid	EggPC	DOPC	DOPC:cholesterol	SOPC
h , nm	3.69	3.67	3.90*	3.91
h_e , nm	2.70	2.68	2.91	2.92
$\Delta\psi_c$, mV	920	950	680	1100**
σ_{lys} , mN/m	3.79	4.08	1.89	4.91

Table 1: Values for the total thickness h , the membrane dielectric thickness h_e and the measured critical poration potential $\Delta\psi_c$ for various lipid compositions. The lysis tension σ_{lys} was estimated on the basis of Eq. 8. *The value for h is only approximate because it corresponds to DOPC:cholesterol 4:1 mole fraction. **The value of $\Delta\psi_c$ measured for SOPC was obtained from (4).

From Eqs. 8 and 9, it is clear that vesicles with high initial tension would porate at lower transmembrane potential. For the vesicles made of DOPC:cholesterol 5:1, we observe lower poration threshold as discussed in the main text. Vesicles with this composition, however, did not exhibit higher initial tensions as examined with fluctuation analysis (10) suggesting that the measured critical transmembrane potentials and the estimated lysis tensions were not influenced by the initial tension σ_0 .

From Eqs. 6, 8 and 9, it is obvious that the membrane tension during the pulse evolves with time and has an angular dependence on the tilt angle θ along the vesicle surface. This nonuniform tension does not allow us to apply the theoretical model developed in (1) to the initial stages of pore opening and stabilization in our system. However, with the pores formed in the vesicle, the membrane tension relaxes and thus, it is not expected to influence the slow pore closing stage.

3 Image analysis

The image processing procedure was divided into two stages: membrane detection and pore size measurement.

In the first stage, we performed an image background correction using the background subtraction rolling-ball algorithm (11). We then located the membrane position using a common Sobel edge detector to highlight sharp changes in the intensity. Phase contrast images of sucrose-loaded GUVs in glucose environment show a bright halo around the vesicle, and a dark region in the inner proximity of the bilayer; see the phase contrast snapshots in Fig. 1 in the main text. The membrane is situated at the interface between these two regions, where the amplitude of the intensity gradient is the highest. When the membrane is porated, mixing of solutions occurs in the pore area, leading to lost intensity gradient due to the absence of the bilayer or the presence of a pore. The last step in the membrane detection stage is the conversion of the image to a binary one, whereby the threshold value is calculated using the classical Isodata algorithm (12). In the binary image, the outer white circle corresponds to the boundary between the bright halo surrounding the vesicle and the gray background of the external solution, while the inner one indicates the membrane position; see the binary images in Fig. 1 in the main text. As we consider pores located on the cathode-facing side of the vesicle, in each image we analyzed only the region containing this vesicle hemisphere. The image processing tasks described above were performed with ImageJ (National Institutes of Health, Bethesda, MD).

Pore radius measurements were carried out using an appropriate custom made algorithm, based on cluster detection and distance measurements between extremal cluster pixels. The accuracy of the procedure was checked on several individual cases.

4 Case of several pores

Sometimes, several pores can be created in a single vesicle. Here, we justify the validity of Eq. 5 in this case. Let us assume we have a GUV of size R containing two pores of radii r_1 and r_2 . Eqs. 1 and 3 are thus modified and now read:

$$\frac{\sigma}{\sigma_0} = 1 - \frac{r_1^2}{r_c^2} - \frac{r_2^2}{r_c^2} - \frac{4(R_{in}^2 - R^2)}{r_c^2} \quad (10)$$

and

$$\frac{2\sigma}{3\eta R}(r_1^3 + r_2^3) = -4\pi R^2 \dot{R}. \quad (11)$$

We also have two equations analogous to Eq. 2 for both radii r_1 and r_2 , which leaves us with a set of four equations and four unknowns. Making the assumptions described in section 1, we find the same law for the closure dynamics of both pores. Therefore we conclude that the theoretical model of Brochard-Wyart et al. (1) for the slow closure stage is applicable to vesicles with several pores. This conclusion is indeed supported by the observed linear time dependencies of our data for $R^2 \ln(r)$ for vesicles with more than one pores. It is further corroborated by the coherence and the reproducibility of our results.

5 Decrease in the vesicle size R during electroporation

When exposed to millisecond electric pulses, liposomes can shrink (13). As seen in Fig. 1 in the main text, the vesicle radius can decrease by up to about 10 %. This observation raises the question whether the approximation for constant vesicle radius is reasonable.

Let us denote the initial radius of the GUV before the pulse with R_{in} , and with R_1 and R_2 the vesicle radii at the beginning and at the end of the stage of linear pore closure (LPC), respectively. In the experiments, R_2 was measured to be equal to the final vesicle radius after the pore has completely closed. Inspection of the three radii R_{in} , R_1 and R_2 for all 110 experiments reported in the main text showed that the major decrease in the vesicle size occurs before the LPC stage. In the supplementary Fig. 1 we plotted normalized radii changes for all studied lipid vesicles. Over the whole observation time interval, the vesicle radii decrease by about 7.5 % on the average, while the decrease during the LPC stage is only about 2.2 % on the average. In a large fraction of the measurements (33 out of 110), $R_1 - R_2$ is negative suggesting an increase in the vesicle radius during the LPC stage. However, this scatter, including the negative $R_1 - R_2$ values, is associated with limits imposed by microscopy resolution, i.e, by the accuracy with which the radius is measured. One pixel represents $0.7528 \mu\text{m}$, implying that an error of 1 pixel in the vesicle size measurement leads to a variation of about 4 % for a vesicle with a radius of $20 \mu\text{m}$ (the variation is even higher for smaller vesicles). Thus, the radius change measured during the LPC stage, $R_1 - R_2$, is within the measurement accuracy implying that for

the negative data points, $R_1 - R_2 \cong 0$. Therefore, the vesicle size can be assumed constant during this stage. In the data analysis, we used the values of R_2 for determining the edge tensions.

The error in the determination of the vesicle radius, ΔR , is approximately 2-4 %. The deviation in the measured value of the edge tension arising from this imprecision, $\Delta\gamma$, is then on the order of

$$\frac{\Delta\gamma}{\gamma} = 2\frac{\Delta R}{R} . \quad (12)$$

yielding a relative error of 4-8 % for γ . The standard errors in our experiments were of this order.

References

1. Brochard-Wyart, F., P. de Gennes, and O. Sandre, 2000. Transient pores in stretched vesicles: role of leak-out. *Physica A* 278:32–51.
2. Dimova, R., C. Dietrich, A. Hadjiisky, K. Danov, and B. Pouligny, 1999. Falling ball viscosimetry of giant vesicle membranes: finite-size effects. *Eur. Phys. J. B* 12:589–598.
3. Kinoshita, K., I. Ashikawa, N. Saita, H. Yoshimura, H. Itoh, K. Nagayama, and A. Ikegami, 1988. Electroporation of cell-membrane visualized under a pulsed-laser fluorescence microscope. *Biophys. J.* 53:1015–1019.
4. Needham, D., and R. M. Hochmuth, 1989. Electro-mechanical permeabilization of lipid vesicles - Role of membrane tension and compressibility. *Biophys. J.* 55:1001–1009.
5. Riske, K. A., and R. Dimova, 2005. Electro-deformation and poration of giant vesicles viewed with high temporal resolution. *Biophys. J.* 88:1143–1155.
6. Olbrich, K., W. Rawicz, D. Needham, and E. Evans, 2000. Water permeability and mechanical strength of polyunsaturated lipid bilayers. *Biophys. J.* 79:321–327.
7. Pan, J. J., S. Tristram-Nagle, and J. F. Nagle, 2009. Effect of cholesterol on structural and mechanical properties of membranes depends on lipid chain saturation. *Phys. Rev. E* 80.

8. Nagle, J. F., and S. Tristram-Nagle, 2000. Structure of lipid bilayers. *Biochim. Biophys. Acta* 1469:159–195.
9. Private communications with S. Tristram-Nagle. For more reference sources, see also <http://lipid.phys.cmu.edu/papers08/SummaryofAreas.ppt> .
10. Gracia, R. S., N. Bezlyepkina, R. L. Knorr, R. Lipowsky, and R. Dimova, 2010. Effect of cholesterol on the rigidity of saturated and unsaturated membranes: fluctuation and electrodeformation analysis of giant vesicles. *Soft Matter* 6:1472–1482.
11. Sternberg, S., 1983. Biomedical image processing. *IEEE Comput.* 16:22–34.
12. Ridler, T. W., and S. Calvard, 1978. Picture thresholding using an iterative selection method. *IEEE Trans. Syst. Man. Cybern.* 8:630–632.
13. Portet, T., F. Camps, J.-M. Escoffre, C. Favard, M.-P. Rols, and D. S. Dean, 2009. Visualization of membrane loss during the shrinkage of giant vesicles under electropulsation. *Biophys. J.* 96:4109–4121.

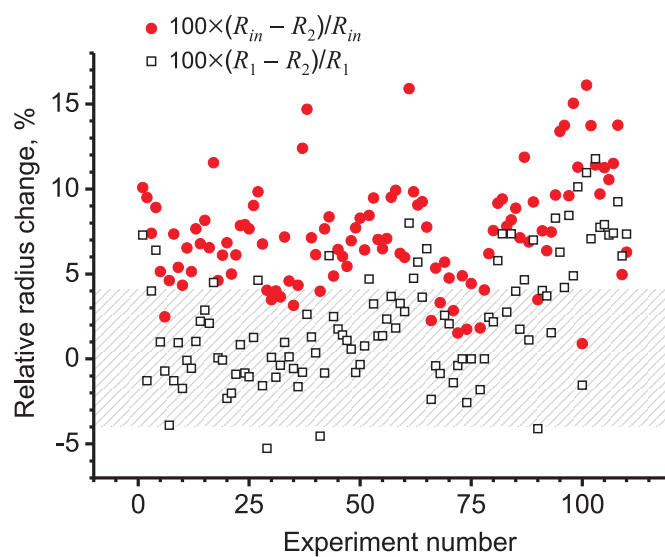


Figure 1: Relative change in the radius of all examined vesicles. The solid circles indicate the radii change in percentage during the whole measured time interval, $100 \times (R_{in} - R_2) / R_{in}$, and the open squares show the relative radii change during the LPC stage only, $100 \times (R_1 - R_2) / R_1$. The shaded area indicates the deviations associated with the error in vesicle radius measurement due to optical resolution. The deviation was evaluated for a vesicle with radius of $20 \mu\text{m}$, see text for details.